

# Entanglement of single-photons and chiral phonons in atomically thin WSe<sub>2</sub>

Xiaotong Chen<sup>1,5</sup>, Xin Lu<sup>1,5</sup>, Sudipta Dubey<sup>1,5</sup>, Qiang Yao<sup>1</sup>, Sheng Liu<sup>2</sup>, Xingzhi Wang<sup>2</sup>, Qihua Xiong<sup>2,3</sup>, Lifa Zhang<sup>4</sup> and Ajit Srivastava <sup>1</sup>

Quantum entanglement is a fundamental phenomenon that, on the one hand, reveals deep connections between quantum mechanics, gravity and spacetime<sup>1,2</sup>, and on the other hand, has practical applications as a key resource in quantum information processing3. Although it is routinely achieved in photon-atom ensembles<sup>4</sup>, entanglement involving solid-state<sup>5-7</sup> or macroscopic objects8 remains challenging albeit promising for both fundamental physics and technological applications. Here, we report entanglement between collective, chiral vibrations in a two-dimensional WSe, host-chiral phonons (CPs)—and single-photons emitted from quantum dots9-13 (QDs) present in it. CPs that carry angular momentum were recently observed in WSe, and are a distinguishing feature of the underlying honeycomb lattice<sup>14,15</sup>. The entanglement results from a 'which-way' scattering process, involving an optical excitation in a QD and doubly-degenerate CPs, which takes place via two indistinguishable paths. Our unveiling of entanglement involving a macroscopic, collective excitation together with strong interactions between CPs and QDs in two-dimensional materials opens up ways for phonon-driven entanglement of QDs and engineering chiral or non-reciprocal interactions at the single-photon level.

Two-dimensional materials with a honeycomb lattice, such as graphene and WSe2, have degenerate, low-energy electronic states that exhibit handedness. In the momentum space, this handedness is identified with the valley pseudo-spin, labelled by the ±K-points of the Brillouin zone, which are related to each other by timereversal symmetry<sup>16,17</sup>. This feature, arising from the presence of two sublattices, is at the heart of 'valley physics' in two-dimensional materials, and has been exploited to create chiral optical excitations using the helicity of incident light<sup>18-20</sup>. Similarly, it has been predicted<sup>15</sup>, and recently observed<sup>14</sup>, that the lattice vibrational modes or phonons in these materials can also have handedness or chirality. Chiral phonons (CPs) in a honeycomb lattice exist both at the centre and the boundary of the Brillouin zone, carrying a (pseudo-) angular momentum of  $l=\pm 1$  along the out-of-plane direction (Fig. 1a). CPs are particularly intriguing as they represent chiral, collective motion of a macroscopic number of atoms as opposed to the chirality of a single charge carrier or an optical excitation. The possibility of chirality-dependent coupling between a single optical excitation and CPs raises the question whether quantum control of the former, which is routinely achieved, can lead to a similar quantum control of collective excitations. Indeed, quantum state preparation, especially entanglement, involving macroscopic objects is not only

a major goal of quantum information technology, but also of fundamental interest, and is being actively pursued in a variety of physical systems<sup>5,21,22</sup>.

Here, we show experimental evidence for entanglement between CPs of monolayer WSe<sub>2</sub> and the corresponding phonon-scattered, single-photons emitted from an embedded quantum dot (QD). The CP modes involve a collective excitation of ~109 atoms of the monolayer as compared to the single optical excitation of the QD. The observed entanglement arises due to (pseudo-)angular momentum selection rules<sup>15</sup> of the phonon-scattering process that correlates the polarization of the single photon with the angular momentum of the doubly degenerate CPs involved. In particular, an exciton in the OD undergoes phonon emission via two indistinguishable paths involving doubly-degenerate CPs with opposite angular momentum. As a result, the state of the emitted photon-phonon system becomes maximally entangled. To demonstrate this entanglement, we analyse the polarization of the photon subsystem, discarding any information of the phonon angular momentum. This results in randomization of the photon polarization, which is determined to be in a completely mixed state with a fidelity of  $99^{+1\%}_{-1.5\%}$ . We emphasize that randomization of polarization is not expected in a coherent scattering process as there is no way for the polarization information to be lost and it arises here as a consequence of an intrinsic lack of knowledge in a 'which-path' scattering. Indeed, the entanglement is destroyed and the polarization recovered once the 'which-path' indistinguishability is removed by an out-of-plane magnetic field that breaks the time-reversal symmetry. This further rules out the possible stochastic nature of the emitted phonon polarization as the reason for randomization of the photon polarization—such a mechanism should not be affected by a magnetic field.

Figure 1a shows the phonon spectra of monolayer WSe<sub>2</sub> calculated using the Quantum Espresso code (see Methods). The optical phonon modes, longitudinal optical/transverse optical (LO/TO) at the  $\Gamma$ -point with an energy of ~20 meV are orthogonal and doubly-degenerate. They transform as E" and can be superposed to get CPs with an angular momentum of  $l=\pm 1^{15}$ . The l=+1 (-1) mode corresponds to a lattice vibration in which the W atoms remain stationary while the Se atoms rotate around them in an anti-clockwise (clockwise) fashion. There are also finite momentum CPs at the  $\pm$ K-points carrying similar angular momentum and these were recently observed by ultrafast spectroscopy<sup>14</sup>. Figure 1b shows Raman spectra measured on WSe<sub>2</sub> samples of different thickness down to a monolayer. Consistent with previous studies<sup>23,24</sup>, we observe a Raman peak corresponding to the CP, E"( $\Gamma$ ), at 176 cm<sup>-1</sup>

<sup>1</sup>Department of Physics, Emory University, Atlanta, GA, USA. <sup>2</sup>Division of Physics and Applied Physics, School of Physical and Mathematical Sciences, Nanyang Technological University, Singapore. <sup>3</sup>NOVITAS, Nanoelectronics Centre of Excellence, School of Electrical and Electronic Engineering, Nanyang Technological University, Singapore, Singapore. <sup>4</sup>Center for Quantum Transport and Thermal Energy Science, School of Physics and Technology, Nanjing Normal University, Nanjing, China. <sup>5</sup>These authors contributed equally. Xiaotong Chen, Xin Lu, Sudipta Dubey. \*e-mail: ajit.srivastava@emory.edu

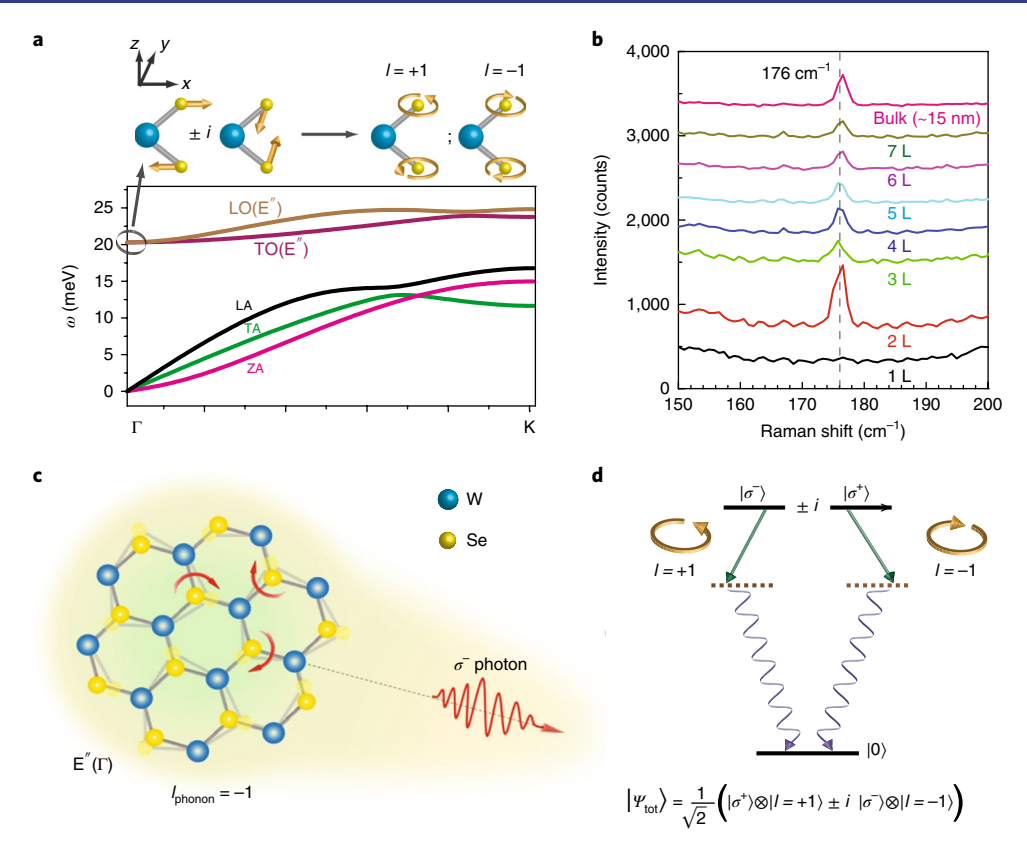


**Fig. 1** | Chiral phonons and phonon-photon entanglement. **a**, Calculated phonon dispersion of monolayer WSe<sub>2</sub> along the Γ-K direction of the Brillouin zone. CPs with (pseudo-)angular momentum  $I=\pm 1$  occur at the zone centre (Γ-point) and the zone boundary (±K-points). The acoustic branches labelled LA, TA and ZA correspond to longitudinal, transverse and out-of-plane modes, respectively. Top, vibrational normal modes of the doubly-degenerate E"(Γ) mode in monolayer WSe<sub>2</sub>. Whereas W atoms remain stationary, the vibration of Se atoms can be chosen in any in-plane direction. Superposition of two orthogonal linear vibrations results in chiral phonons with clockwise or anti-clockwise motion. **b**, Raman spectra of the E"(Γ) mode in WSe<sub>2</sub> of different thickness. The energy of E"(Γ) is measured to be 176 cm<sup>-1</sup> (21.8 meV). The peak is forbidden in a monolayer due to symmetry constraints. **c,d**, Schematic of phonon-photon entanglement. The circularly polarized states ( $\sigma^+/\sigma^-$ ) with an angular momentum of I=+1/-1 are degenerate in WSe<sub>2</sub> due to time-reversal symmetry. The I=+1 (-1) phonon can only couple a  $\sigma^-(\sigma^+)$  photon to a scattered photon with angular momentum of I=+1 (-1) due to conservation of angular momentum. The indistinguishability of the two paths in this 'which-way' scattering process leads to entanglement of the phonon and the photon.

or 21.8 meV, which is in very good agreement with the calculations. The Raman peak is not observed in the monolayer sample due to symmetry considerations that forbid it (see Supplementary Information).

Figure 1c,d shows the basic idea behind entanglement of a CP with an optical excitation. Consider an optical excitation with in-plane linear polarization  $(\pi^{\rm v}/\pi^{\rm v})$ , for example, arising from an anisotropic potential that defines a preferred direction of the in-plane polarization, coupled to CPs through electron–phonon coupling. The optical excitation can be considered to be a superposition of left and right circularly polarized  $(\sigma^+/\sigma^-)$  states that carry an angular momentum of  $\pm 1$  along the out-of-plane direction. Due to conservation of angular momentum in a three-fold symmetric crystal 15, the l=+1 (-1) phonon couples only with  $\sigma^-$  ( $\sigma^+$ ) photon, as shown in Fig. 1d (see Supplementary Information). In other words, due to the degeneracy of phonons, the photon states involved in the superposition can scatter by two indistinguishable paths, with angular momentum conservation correlating the states of their polarization. As a result, after the scattering process, the state of the phonon–photon is

$$|\varPsi_{\rm tot}\rangle = \frac{1}{\sqrt{2}} \left[ |\sigma^{+}\rangle \otimes |l_{\rm phonon} \! = \! +1\rangle \pm i \ |\sigma^{-}\rangle \otimes |l_{\rm phonon} \! = \! -1\rangle \right] \eqno(1)$$

where the  $\pm$  sign follows from the  $\pi^x/\pi^y$  polarization of the incoming photon and  $\sigma^+/\sigma^-$  labels the helicity of the out-going photon.

This state is nothing other than a maximally entangled state of a phonon-photon system.

To realize the entanglement outlined above, we make use of the fact that a localized neutral exciton ( $X^0$ ) in a WSe<sub>2</sub> QD<sup>25–27</sup> is split into two orthogonal linearly polarized states due to an anisotropic electron–hole exchange interaction<sup>9–12</sup>. Indeed, this fine-structure splitting is a hallmark of localized  $X^0$  in many QD systems, including self-assembled GaAs QDs<sup>28</sup>. The use of QDs should also enhance the electron–phonon coupling due to quantum confinement effects and lower the symmetry to allow CP-scattering even in monolayer crystals (see Supplementary Information).

We perform polarization-resolved photoluminescence (PL) spectroscopy on a monolayer WSe<sub>2</sub> sample in a field effect transistor device at low incidence powers (see Methods). As shown in Fig. 2a, at positive gate voltage ( $V_{\rm g} \sim +20\,{\rm V}$ ) when the sample is electron-doped, we observe the attractive Fermi-polaron peak ( $X_{\rm ap}$ )<sup>29</sup> while for  $-90\,{\rm V} < V_{\rm g} < 20\,{\rm V}$ , a faint free-exciton peak (X<sup>0</sup>) is visible. Around  $V_{\rm g} = 20\,{\rm V}$ , the so-called defect peak (D) appears and dominates the PL signal. Remarkably, this coincides very well with the appearance of sharp QD peaks at lower energies than D, showing that the QDs originate from the WSe<sub>2</sub> monolayer.

Figure 2b shows PL spectra, focusing on a few QD-like peaks. At  $V_{\rm g}\!\sim\!-23\,\rm V$ , when the sample is depleted of electrons, two set of doublets, labelled D3a and D3b, appear simultaneously. Moreover, the two doublets wander spectrally in an identical manner, as

NATURE PHYSICS LETTERS

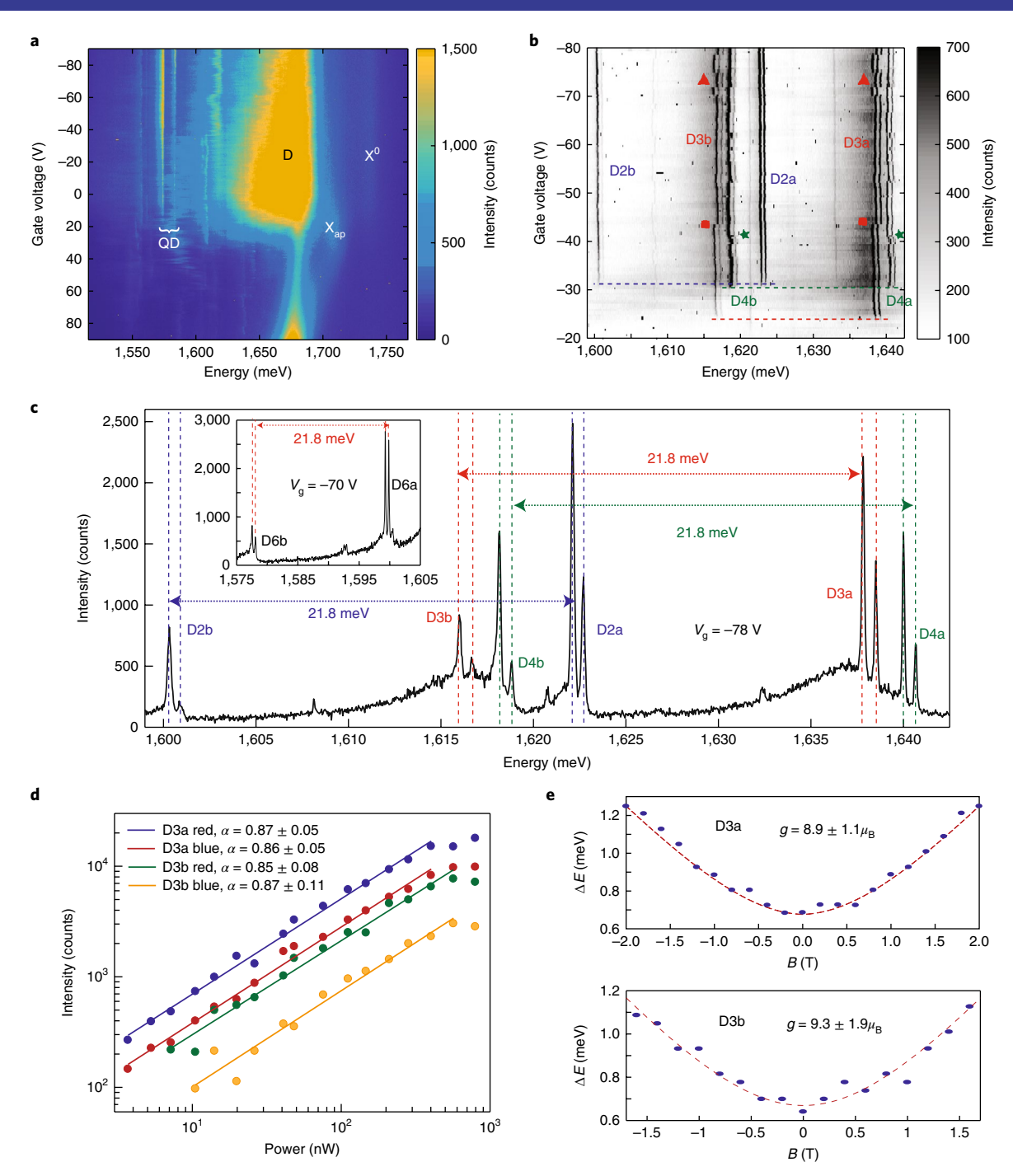


**Fig. 2 | QDs and their phonon replicas in monolayer WSe<sub>2</sub>. a**, PL intensity map as a function of  $V_g$ . The attractive Fermi-polaron peak ( $X_{ap}$ ) and the free exciton X<sup>0</sup> are identified. The defect peak (D) is observed when  $-90 \text{ V} < V_g < 20 \text{ V}$ , and concurrently sharp QD-like peaks appear with energy lower than D. **b**, Gate-dependent PL intensity map of QDs. The assignment of a QD group is based on the correlated spectral jittering pattern highlighted in **b**: green stars for the D4 group; red triangles and squares for the D3 group. Each group contains two doublets, with the high- and low-energy doublets named as a and b (for example, D3a and D3b), respectively. The dashed line indicates the onset  $V_g$  for each group. **c**, A cross-sectional PL spectrum at  $V_g = -78 \text{ V}$ . The splitting energy of the a doublets is identical to that of the corresponding b doublets. The energy spacing between the a and b doublets is 21.8 meV, which is consistent with the energy of the E"(Γ) phonon. Inset shows similar behaviour for the QD D6. **d**, Power dependence plot of the D3 group. The lines are the power-law fitting  $I \propto P^{\alpha}$ . The extracted values of  $\alpha$  are the same within the standard deviation for the four peaks in the D3 group. The sub-linear dependence further confirms the sharp peaks are related to trapped excitons. **e**, Zeeman splitting between the two peaks in the D3a (top) and D3b (bottom) doublets as a function of *B*. The *g*-factors are same for both doublets within the error bar. **d** and **e** were measured at  $V_g = -80 \text{ V}$ .  $\mu_B$  is the Bohr magneton.

highlighted by the solid symbols. Consequently, we identify D3a and D3b as originating from the same QD (namely, D3). Furthermore, the D2a/D2b and D4a/D4b pairs of doublets exhibit similar behaviour in their turn-on voltage and spectral wandering, and are

assigned to the QDs D2 and D4, respectively. Figure 2c shows cross-sectional PL spectra at a fixed  $V_{\rm g}$ . We first notice that the energy splitting of the a doublets is identical to that of the corresponding b doublets. Moreover, the energy spacing between the a and b peaks

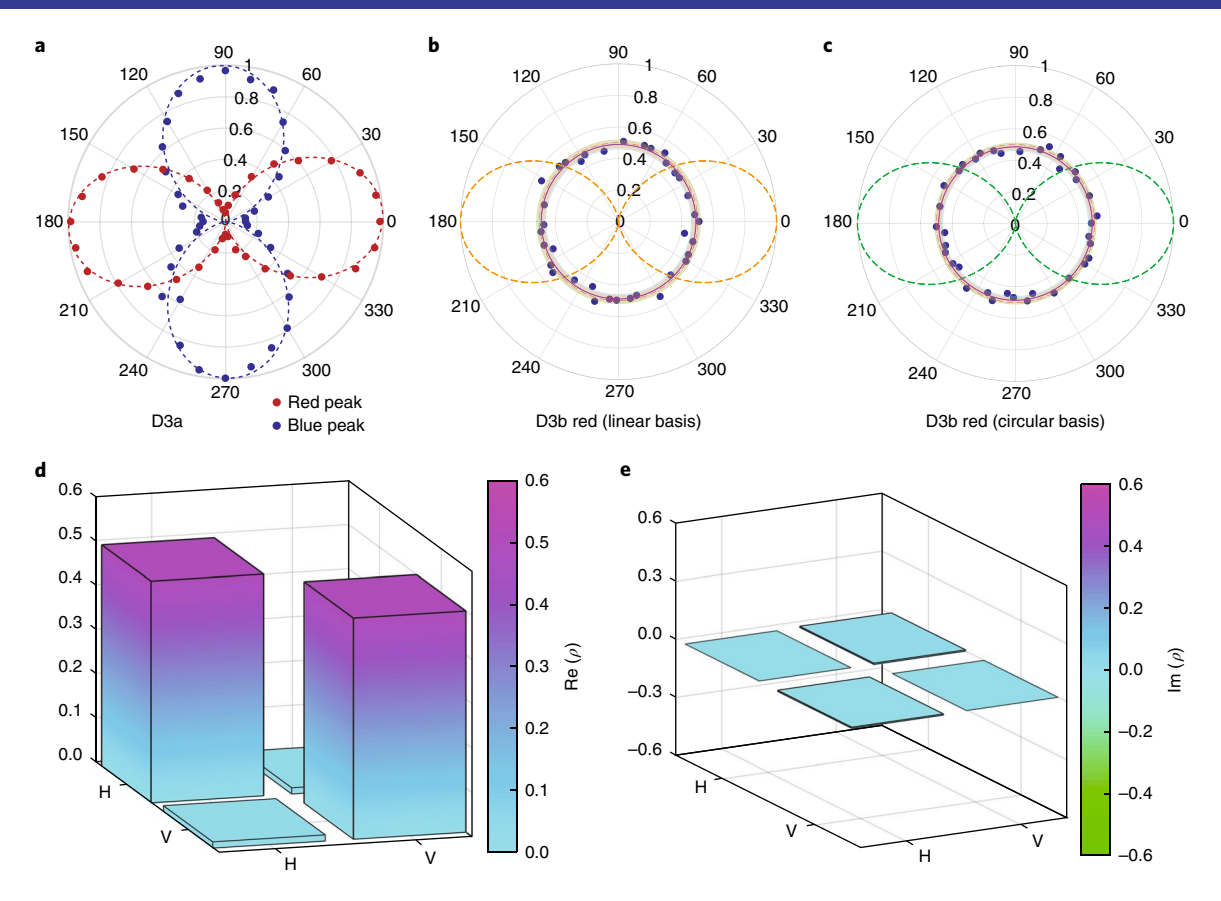


**Fig. 3** | **Polarization dependence of QDs and their phonon replicas in monolayer WSe<sub>2</sub>. a**, Polarization of the D3a doublet measured in the linear basis. The lines are  $\sin^2\theta/\cos^2\theta$  fits to the experimental data (dots), showing the two peaks are cross-polarized. **b,c**, Polarization of the red peak from the D3b doublet in the linear (**b**) and circular (**c**) bases. Black lines are the average values, and the brown shaded regions represent the standard deviation of the experimental data (dots). The orange dashed line in **b** shows an example of the linearly polarized emission in the linear basis measurement. The red dashed circle with a radius of 0.5 can be either circularly polarized emission or an unpolarized light source. Further measurements in the circular basis (**c**) distinguish unpolarized emission from circular polarization. The green dashed line in **c** shows an example of circularly polarized emission in a circular basis measurement while the red dashed circle with a radius of 0.5 represents unpolarized emission. **d,e**, Real (**d**) and imaginary (**e**) parts of the density matrix for the polarization state of the D3b red peak. The value of 0.5 for the diagonal matrix elements corresponds to a completely mixed state. Polarization measurements were carried out at  $V_a = -80 \text{ V}$ .

for all the three QDs is precisely 21.8 meV. As this energy spacing is exactly equal to the measured energy of the  $E''(\Gamma)$  phonon in the Raman spectra (Fig. 1b), we conclude that the lower-energy b peaks are the chiral phonon replica of the parent a peaks. Moreover, the a peaks being doublets is consistent with a localized  $X^0$ , and the corresponding fine-structure splitting of  ${\sim}600\,\mu\text{eV}$  is in excellent agreement with previous studies  $^{9-13}$ . We observe this behaviour in several other QDs (see Supplementary Information).

To further confirm that the b peaks are indeed phonon replicas and not other excitonic complexes such as biexcitons<sup>30</sup> or evenly charged excitons, we first determine the excitation power dependence of all the peaks, as shown in Fig. 2d. All the peaks exhibit a sub-linear, power-law behaviour with the emission intensity (I) scaling with the incident power (P) as  $P^a$ , with  $\alpha \sim 0.8$ , thus ruling out biexcitons as a possible origin of the b peaks. Figure 2e shows that both the a and b doublets exhibit Zeeman splitting in an out-of-plane magnetic field (B) with almost identical g-factors, as is expected for the parent and phonon replica peaks. The measured value of the g-factor (approximately 9) is consistent with previous studies of QDs in WSe<sub>2</sub><sup>9-13</sup>. We note that the ratio of the intensity of the phonon replica to the parent peak, which quantifies the strength of the exciton–phonon coupling and is called the Huang–Rhys factor, varies from S = 0.2 to 0.9 (see Supplementary

Information) and is more than an order of magnitude larger than for GaAs-based QDs<sup>31</sup>.

Having established that we observe a strong phonon replica (b doublets) of the localized neutral exciton (a doublets) with the phonon involved being the  $E''(\Gamma)$  CP, we analyse the polarization properties of the doublets. Figure 3a shows that the red and blue peaks of the D3a parent peak are linearly polarized and orthogonal to each other. This is consistent with the D3a doublet's assignment as a localized  $X^0$ . Similar linearly polarized emission is observed for other a peaks as well (see Supplementary Information). However, the b peaks, in spite of being phonon replicas and inheriting all their properties from the parent a peaks, show completely unpolarized emission in both linear and circular basis measurements (Fig. 3b,c). This stark difference in the polarization property of the phonon replica with respect to the parent peak is particularly puzzling given the coherent nature of the Raman-like phonon emission.

To explain this anomaly, we first recall that the phonons involved in the scattering process giving rise to the replicas are doubly-degenerate, orthogonal CPs with  $l_{\rm phonon} = \pm 1$ . Moreover, the linearly polarized localized  $X^0$  can be thought of as a superposition of  $\sigma^+$  and  $\sigma^-$  photons, and we have a situation identical to that illustrated in Fig. 1d. As a consequence, the combined state of the emitted phonon and replica photon system after the scattering is maximally

NATURE PHYSICS LETTERS

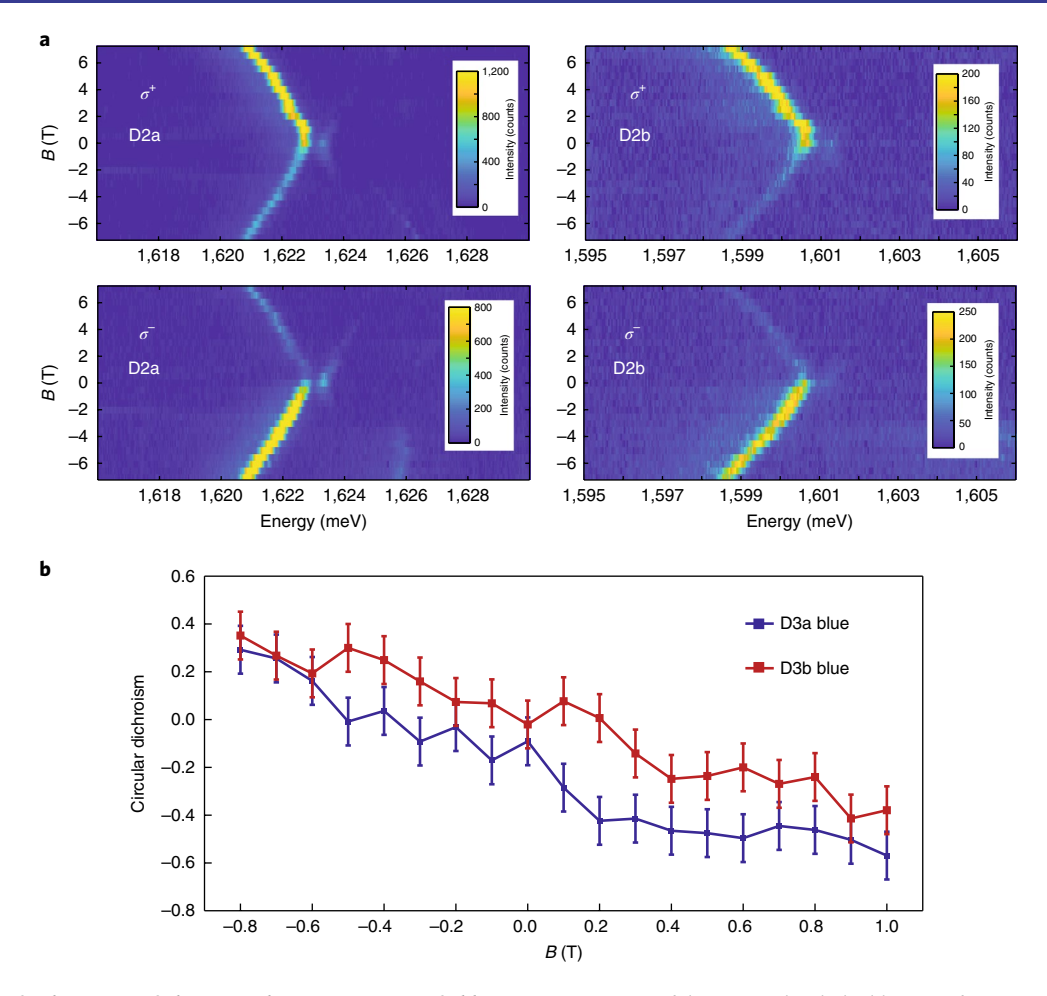


**Fig. 4 | Recovery of polarization of phonon replicas in a magnetic field. a**, PL intensity map of the D2a and D2b doublets as a function of B measured in the circular basis. As the out-of-plane B field increases, the splitting between the two peaks comprising the doublets A and A increases. Efficient thermalization results in only the low-energy peak being visible in the PL. In addition, the intensity of the D2a red peak increases in the A configuration, whereas it decreases in the A configuration (left). The D2b red peak shows the same trend of behaviour (right). **b**, Circular dichroism of the D3a blue peak and the D3b blue peak as a function of A. The circular polarization of D3b is smaller than D3a in the range from A0.8 to 1T. Under A0 field, Circular dichroism of the D3b peak recovers from zero and follows that of the D3a peak. Measurements were carried out at A1 to A2 and A3 field, Circular dichroism of the D3b peak recovers from zero and follows that of the D3a peak. Measurements were carried out at A3 to 1T. Under A4 field, Circular dichroism of the D3b peak recovers from zero and follows that of the D3a peak. Measurements were carried out at A3 to 2T. The error bars are obtained by calibrating the optical set-up using linearly polarized light and arise due to imperfections in the polarization optics.

entangled. As we measure only the polarization of the replica photon and do not have access to the information of phonon angular momentum, we must trace out the phonon subsystem to find the state of the photon after it is measured. Starting with the maximally entangled state of equation (1) and making use of the fact that the two phonon states with opposite angular momentum are orthogonal, we obtain for the photon subsystem,

$$|\psi_{\text{photon}}\rangle = \frac{1}{2} (|\sigma^{+}\rangle \langle \sigma^{+}| + |\sigma^{-}\rangle \langle \sigma^{-}|)$$
 (2)

which is a completely mixed state of polarization, independent of the basis.

In other words, the information of the polarization of the parent peak photon is lost with the phonon that we never measure. Owing to entanglement, the measurement of the phonon angular momentum to be, say l=+1 (l=-1), would simultaneously project the polarization of the replica photon to the  $\sigma^+$  ( $\sigma^-$ ) state. However, such a measurement of phonon angular momentum is challenging and is left for future experiments. In reality, the emitted CP has a finite lifetime of tens of picoseconds, after which it decays into other lower-energy phonon modes due to anharmonicity of the

lattice potential<sup>32</sup>. This decay can be thought of as a measurement of the phonon subsystem of the entangled state, but as the outcome of this measurement is irreversibly lost to the lattice and environment, the photon subsystem is projected to a completely unpolarized state.

Figure 3d,e shows a quantitative comparison of the measured photon polarization to a completely mixed state of polarization. By extracting the Stokes parameter from the polarization measurements we reconstruct the density matrix of the photon polarization and estimate a fidelity of  $\mathcal{F}=99^{+1.9}_{-1.5\%}$  to the completely mixed state. Other QDs exhibit similar polarization behaviour and high values of fidelity (see Supplementary Information).

The entanglement scheme described above relies crucially on two sets of degeneracies: that of the two  $\sigma$ -polarized states entering the superposition to give linearly polarized light and that of the orthogonal CPs. These degeneracies lead to two indistinguishable paths for the scattering to take place, which have a definite phase relationship in their probability amplitudes and hence result in the entangled state. Consequently, if any or both of these degeneracies are lifted, one expects the paths to be become distinguishable and the entanglement to be destroyed. Although both the degeneracies are protected by time-reversal symmetry, it is difficult to break the CP degeneracy as phonons do not couple well to B in

non-magnetic materials such as WSe<sub>2</sub>. However, the degeneracy of the  $\sigma$ -polarized states can be broken by an out-of-plane B in a valley Zeeman-like effect<sup>33,34</sup>.

Figure 4a shows the *B* dependence of the polarization of the parent and the replica peak analysed in a circular basis. As *B* increases, the electron–hole exchange in the  $X^0$  doublet is overcome and it becomes  $\sigma$ -polarized. We observe that the replica peak recovers its polarization and becomes  $\sigma$ -polarized with increasing *B*, closely following the behaviour of the parent peak (Fig. 4b). The recovery of polarization is consistent with the entanglement scheme described above and rules out other mechanisms such as the phonon polarization being oriented in arbitrary directions during the emission events. As the phonon emission process is not expected to be affected by the weak *B* used in our experiments, such a mechanism would imply unpolarized photon emission even under magnetic fields, contrary to our observations.

The angular momentum selection rules of Fig. 1d predict a reversal in helicity of the phonon replica with respect to the parent peak. In fact, we do observe a reversal in helicity for the  $E''(\Gamma)$  mode in non-resonant Raman scattering measurements (see Supplementary Information). However, the polarization of the phonon replica is to a large degree co-polarized with that of the parent peak at finite B (Fig. 4). Although we lack understanding of this behaviour and further studies are needed to address it, similar behaviour has been reported by several groups for Raman scattering involving CPs. It was found that the helicities of the incident photon and the Raman scattered photon are reversed with respect to each other only when the incident photon energy is far detuned from the free exciton resonance, whereas they are co-polarized for a quasi-resonant excitation<sup>35–37</sup>. In the case of the phonon replica of the QD emission, the role of the laser is played by the parent peak photon while the Raman scattered photon is the replica photon and the relevant resonance is the X<sup>0</sup> QD transition. Thus, for the phonon replica process, we are always 'on-resonance' with respect to the relevant resonance of the QD transition and our situation is closer to the quasi-resonant case of Raman scattering, consistent with previous studies.

Our findings lay the groundwork for the realization of quantumoptomechanical platforms in van der Waals materials<sup>38</sup>. The strong single exciton–phonon coupling in QDs of two-dimensional materials shown here can serve as a source of single, CPs. Future studies can exploit this chiral coupling to manipulate the quantum state of the collective excitation by an all-optical control of the QD or couple two different QDs via a single CP mode. Furthermore, the chirality of a macroscopic mode is an intriguing possibility that has potential for engineering non-reciprocal interactions at the quantum level.

# Online content

Any methods, additional references, Nature Research reporting summaries, source data, statements of data availability and associated accession codes are available at https://doi.org/10.1038/s41567-018-0366-7.

Received: 27 August 2018; Accepted: 6 November 2018; Published online: 10 December 2018

# References

- Maldacena, J. & Susskind, L. Cool horizons for entangled black holes. Fortschr. Phys. 61, 781–811 (2013).
- Cao, C., Carroll, S. M. & Michalakis, S. Space from Hilbert space: recovering geometry from bulk entanglement. *Phys. Rev. D* 95, 024031 (2017).
- Nielsen, M. A. & Chuang, I. L. Quantum Computation and Quantum Information: 10th Anniversary Edition (Cambridge Univ. Press, Cambridge, 2010).
- Moehring, D. L. et al. Entanglement of single-atom quantum bits at a distance. *Nature* 449, 68–71 (2007).
- Gao, W. B., Fallahi, P., Togan, E., Miguel-Sanchez, J. & Imamoğlu, A. Observation of entanglement between a quantum dot spin and a single photon. *Nature* 491, 426–430 (2012).

- De Greve, K. et al. Quantum-dot spin-photon entanglement via frequency downconversion to telecom wavelength. *Nature* 491, 421–425 (2012).
- Dolde, F. et al. Room-temperature entanglement between single defect spins in diamond. Nat. Phys. 9, 139–143 (2013).
- Lee, K. C. et al. Entangling macroscopic diamonds at room temperature. Science 334, 1253–1256 (2011).
- Srivastava, A. et al. Optically active quantum dots in monolayer WSe<sub>2</sub>. Nat. Nanotech. 10, 491–496 (2015).
- Koperski, M. et al. Single photon emitters in exfoliated WSe<sub>2</sub> structures. Nat. Nanotech. 10, 503–506 (2015).
- Chakraborty, C., Kinnischtzke, L., Goodfellow, K. M., Beams, R. & Vamivakas, A. N. Voltage-controlled quantum light from an atomically thin semiconductor. *Nat. Nanotech.* 10, 507–511 (2015).
- He, Y.-M. et al. Single quantum emitters in monolayer semiconductors. Nat. Nanotech. 10, 497–502 (2015).
- Tonndorf, P. et al. Single-photon emission from localized excitons in an atomically thin semiconductor. Optica 2, 347–352 (2015).
- 14. Zhu, H. et al. Observation of chiral phonons. Science 359, 579-582 (2018).
- Zhang, L. & Niu, Q. Chiral phonons at high-symmetry points in monolayer hexagonal lattices. *Phys. Rev. Lett.* 115, 115502 (2015).
- Xu, X., Yao, W., Xiao, D. & Heinz, T. F. Spin and pseudospins in layered transition metal dichalcogenides. *Nat. Phys.* 10, 343–350 (2014).
- Xiao, D., Liu, G.-B., Feng, W., Xu, X. & Yao, W. Coupled spin and valley physics in monolayers of MoS<sub>2</sub> and other group-VI dichalcogenides. *Phys. Rev. Lett.* 108, 196802 (2012).
- Mak, K. F., He, K., Shan, J. & Heinz, T. F. Control of valley polarization in monolayer MoS<sub>2</sub> by optical helicity. *Nat. Nanotech.* 7, 494–498 (2012).
- Zeng, H., Dai, J., Yao, W., Xiao, D. & Cui, X. Valley polarization in MoS<sub>2</sub> monolayers by optical pumping. *Nat. Nanotech.* 7, 490–493 (2012).
- Cao, T. et al. Valley-selective circular dichroism of monolayer molybdenum disulphide. Nat. Commun. 3, 887 (2012).
- DiCarlo, L. et al. Preparation and measurement of three-qubit entanglement in a superconducting circuit. *Nature* 467, 574–578 (2010).
- Steffen, M. et al. Measurement of the entanglement of two superconducting qubits via state tomography. Science 313, 1423–1425 (2006).
- Luo, X. et al. Effects of lower symmetry and dimensionality on Raman spectra in two-dimensional WSe<sub>2</sub>. Phys. Rev. B 88, 195313 (2013).
- Kim, S., Kim, K., Lee, J.-U. & Cheong, H. Excitonic resonance effects and Davydov splitting in circularly polarized Raman spectra of few-layer WSe<sub>2</sub>. 2D Mater. 4, 045002 (2017).
- Branny, A., Kumar, S., Proux, R. & Gerardot, B. D. Deterministic straininduced arrays of quantum emitters in a two-dimensional semiconductor. *Nat. Commun.* 8, 15053 (2017).
- Palacios-Berraquero, C. et al. Atomically thin quantum light-emitting diodes. Nat. Commun. 7, 12978 (2016).
- Palacios-Berraquero, C. et al. Large-scale quantum-emitter arrays in atomically thin semiconductors. Nat. Commun. 8, 15093 (2017).
- Gammon, D., Snow, E. S., Shanabrook, B. V., Katzer, D. S. & Park, D. Fine structure splitting in the optical spectra of single GaAs quantum dots. *Phys. Rev. Lett.* 76, 3005–3008 (1996).
- Sidler, M. et al. Fermi polaron-polaritons in charge-tunable atomically thin semiconductors. Nat. Phys. 13, 255–261 (2016).
- He, Y.-M. et al. Cascaded emission of single photons from the biexciton in monolayered WSe<sub>2</sub>. Nat. Commun. 7, 13409 (2016).
- Heitz, R., Mukhametzhanov, I., Stier, O., Madhukar, A. & Bimberg, D. Enhanced polar exciton-LO-phonon interaction in quantum dots. *Phys. Rev. Lett.* 83, 4654–4657 (1999).
- Cai, Y., Lan, J., Zhang, G. & Zhang, Y.-W. Lattice vibrational modes and phonon thermal conductivity of monolayer MoS<sub>2</sub>. *Phys. Rev. B* 89, 035438 (2014).
- Srivastava, A. et al. Valley Zeeman effect in elementary optical excitations of monolayer WSe<sub>2</sub>. Nat. Phys. 11, 141–147 (2015).
- Aivazian, G. et al. Magnetic control of valley pseudospin in monolayer WSe<sub>2</sub>. Nat. Phys. 11, 148–152 (2015).
- Chen, S.-Y., Zheng, C., Fuhrer, M. S. & Yan, J. Helicity-resolved Raman scattering of MoS<sub>2</sub>, MoSe<sub>2</sub>, WS<sub>2</sub>, and WSe<sub>2</sub> atomic layers. *Nano. Lett.* 15, 2526–2532 (2015).
- Drapcho, S. G. et al. Apparent breakdown of Raman selection rule at valley exciton resonances in monolayer MoS<sub>2</sub>. Phys. Rev. B 95, 165417 (2017).
- Yoshikawa, N., Tani, S. & Tanaka, K. Raman-like resonant secondary emission causes valley coherence in CVD-grown monolayer MoS<sub>2</sub>. *Phys. Rev.* B 95, 115419 (2017).
- Geim, A. K. & Grigorieva, I. V. Van der Waals heterostructures. Nature 499, 419–425 (2013).

## Acknowledgements

We acknowledge many enlightening discussions with A. Imamoğlu, W. Gao and M. Kroner. We also acknowledge technical help from T. Neal and E. Liu. A.S. acknowledges support from Emory University startup funds and the National Science

NATURE PHYSICS LETTERS

Foundation through the EFRI Program grant number EFMA-1741691. L.Z. thanks M. Gao for helpful calculations and discussions, and acknowledges support from the National Natural Science Foundation of China (grant No. 11574154). Q.X. gratefully acknowledges strong support from the Singapore National Research Foundation via an NRF-ANR joint grant (NRF2017-NRF-ANR002 2D-Chiral) and the Singapore Ministry of Education via an AcRF Tier2 grant (MOE2017-T2-1-040) and Tier1 grants (RG 113/16 and RG 194/17)

# **Author contributions**

X.C., X.L., S.D. and Q.Y. carried out the quantum dot measurements and S.L. measured the Raman data. X.L. and X.W. prepared the samples. A.S., L.Z. and Q.X. supervised the project. All authors were involved in analysis of the experimental data and contributed extensively to this work.

# **Competing interests**

The authors declare no competing interests.

# **Additional information**

 $\label{eq:supplementary} \textbf{Supplementary information} \ is \ available \ for \ this \ paper \ at \ https://doi.org/10.1038/s41567-018-0366-7.$ 

Reprints and permissions information is available at www.nature.com/reprints.

Correspondence and requests for materials should be addressed to A.S.

**Publisher's note:** Springer Nature remains neutral with regard to jurisdictional claims in published maps and institutional affiliations.

© The Author(s), under exclusive licence to Springer Nature Limited 2018

# Methods

Sample fabrication. Monolayer WSe $_2$  is mechanically exfoliated from the bulk WSe $_2$  crystal (HQ Graphene) on polydimethylsiloxane (PDMS). Similarly thin hexagonal boron nitride (hBN) flake (hBN crystal from HQ Graphene) is exfoliated on a degenerately doped Si (Si<sup>++</sup>) substrate with a 285 nm SiO $_2$  layer on top. The fabrication of the WSe $_2$ /BN/SiO $_2$  stack is done via the PDMS-based dry transfer method<sup>19</sup>. Electron beam lithography is used to deposit 30 nm Pd/80 nm Au metal contacts on WSe $_2$ , which act as the source and drain electrodes. The charge carrier density in WSe $_2$  is controlled by applying a voltage (Keithley 2400 Sourcemeter) to the Si<sup>++</sup> substrate, with the 285 nm SiO $_2$  layer acting as the gate dielectric.

PL spectroscopy. The sample is loaded into a closed-cycle cryostat (BlueFors) equipped with a magnetic field ranging from -8 to +8 T and cooled down to ~3.5 K. A piezo controller (Attocube Systems) is used to position the sample. PL spectroscopy was performed using a home-built confocal microscope set-up. The emission was collected using an aspheric lens (numerical aperture 0.55) and directed to a high-resolution (focal length: 750 mm) spectrometer where it was dispersed by a 1,200 grooves per mm or 300 grooves per mm grating (both blazed at 750 nm). A liquid nitrogen-cooled charge coupled device (Princeton Instruments SP-2750, PyLoN 1340 × 400 pixels CCD) was used as the detector. Two excitation sources are used: a HeNe laser at a wavelength of 632.8 nm with a power of 4 µW or a mode-hop-free tunable continuous-wave Ti:Sapphire laser (M Squared) with resolution of 0.1 pm and a power of 300 nW. The spot sizes for the Ti:Sapphire laser and the HeNe laser are  $\sim 1 \, \mu m$  and  $\sim 2-5 \, \mu m$ , respectively. The wavelength of the Ti:Sapphire laser is tuned for resonance to the localized excitons to increase the QD emission intensity. The polarization of the incident laser is controlled using a polarizer together with a half- and quarter-wave plate. Polarization measurements were performed by means of a Wollaston prism that separates light into the s and p components. A quarter-wave plate is placed after the Wollaston prism to convert

the linearly polarized light into a circularly polarized signal, so that the signal will be insensitive to the grating efficiency. A half-wave (super-achromatic 600-2.700 nm, Thorlabs) or a quarter-wave (zero order @ 780 nm) plate is placed before the Wollaston prism for the linear or circular basis measurement. The influence of blinking on polarization measurements is eliminated in this set-up (see Supplementary Information). In all the magnetic field dependence measurements, B is applied perpendicular to the plane of the sample.

Raman spectroscopy. Raman scattering measurements were carried out at room temperature. The excitation source is a He-Cd laser at a wavelength of 441.6 nm with a power of 0.5 mW. The backscattered signal was collected through a 100× objective, directed to a micro-Raman spectrometer (Horiba-HR Evo), where it was dispersed by a 1,800 grooves per mm grating, and finally detected using a liquid nitrogen cooled charge-coupled device with a spectral resolution of ~1 cm<sup>-1</sup>.

**Phonon dispersion calculation.** We use Quantum Espresso Code to calculate the phonon dispersion of monolayer WSe<sub>2</sub>. The norm-conserving pseudopotential within the local density approximation of Perdew–Zunger is used. The kinetic energy cutoff for charge density is 260 Ry. The first Brillouin zone is sampled with a  $31 \times 31 \times 1$  Monkhorst–Pack grid. The vacuum region thickness is 20 Å. The optimized equilibrium lattice constant of monolayer WSe, is 3.13 Å.

# Data availability

The data that support the plots within this paper and other findings of this study are available from the corresponding author upon reasonable request.

### References

 Castellanos-Gomez, A. et al. Deterministic transfer of two-dimensional materials by all-dry viscoelastic stamping. 2D Mater. 1, 011002 (2014).